GEOPHYSICS, VOL. 74, NO. 5 (SEPTEMBER-OCTOBER 2009); P. E193–E203, 11 FIGS., 4 TABLES.
10.1190/1.3183940

Exploring trends in microcrack properties of sedimentary rocks: An audit of dry-core velocity-stress measurements

Doug A. Angus[1], James P. Verdon[2], Quentin J. Fisher[1], and J.-M. Kendall[2]

ABSTRACT

Rock-physics models are used increasingly to link fluid and mechanical deformation parameters for dynamic elastic modeling. We explore the input parameters of an analytical stress-dependent rock-physics model. To do this, we invert for the stress-dependent microcrack parameters of more than 150 sedimentary rock velocity-stress core measurements taken from a literature survey. The inversion scheme is based on a microstructural effective-medium formulation defined by a second-rank crack-density tensor (scalar crack model) or by a second- and fourth-rank crack-density tensor (joint inversion model). Then the inversion results are used to explore and predict the stress-dependent elastic behavior of various sedimentary rock lithologies using an analytical microstructural rock-physics model via the initial model input parameters: initial crack aspect ratio and initial crack density. Estimates of initial crack aspect ratio are consistent among most lithologies with a mean of 0.0004, but for shales they differ up to several times in magnitude with a mean of 0.001. Estimates of initial aspect ratio are relatively insensitive to the inversion method, although the scalar crack inversion becomes less reliable at low values of normal-to-tangential crack compliance ratio (B_N/B_T). Initial crack density is sensitive to the degree of damage as well as the inversion procedure. An important implication is that the fourth-rank crack-density term is not necessarily negligible for most sedimentary rocks and evaluation of this term or B_N/B_T is necessary for accurate prediction of initial crack density. This is especially important because recent studies suggest that B_N/B_T can indicate fluid content in cracks.

INTRODUCTION

Seismic monitoring of petroleum reservoirs has been used to image fluid compartmentalization and movement, stress redistribution, natural-fracture distribution, and hydraulic-fracture formation. Time-lapse seismic monitoring is used to infer changes in pore pressure/stress and saturation within reservoirs and surrounding rock mass (e.g., Calvert, 2005). However, analysis of time-lapse results is complicated by the relative nonuniqueness of relating changes in seismic attributes (e.g., traveltime and acoustic impedance) to changes in reservoir-fluid saturation and pore pressure. Although the interpretation of time-lapse seismic data is influenced heavily by reservoir complexity (e.g., geometry), a significant source of ambiguity in seismic analyses stems from the uncertainty in relating perturbations in seismic velocities with stress/strain-induced changes in the rock-physics properties.

Recent studies focus on applying coupled fluid-flow and geomechanical modeling to enhance predictions of the subsurface response to fluid extraction and/or injection (e.g., Dean et al., 2005). Predicting the seismic response based on results from coupled fluid-flow and geomechanical modeling can improve our understanding of the relationship between seismic attributes and changes in fluid properties, stress, and mechanical deformation. However, this requires the use of rock-physics models to link the fluid and mechanical properties of the reservoir system to so-called dynamic elastic (i.e., the elastic response suitable for seismic frequencies) models. Gassmann's equation (see Brown and Korringa, 1975) often is used to explain relative changes in traveltimes and reflection amplitudes from changes in fluid saturation. Yet fluid substitution alone has not been sufficient to explain the temporal and spatial changes in velocities, especially when mechanical deformation occurs within the reservoir and surrounding rock mass (e.g., Hatchell and Bourne, 2005). This is because the elastic behavior of rock is dependent nonlinearly on stress (e.g., Walsh, 1965a, 1965b; Nur and Simmons, 1969).

Various approaches have been developed to account for the influence of stress and strain. For instance, Hatchell and Bourne (2005)

Manuscript received by the Editor 4 November 2008; revised manuscript received 28 April 2009; published online 3 September 2009.
[1]University of Leeds, School of Earth and Environment, Leeds, U. K. E-mail: d.angus@leeds.ac.uk; q.j.fisher@leeds.ac.uk.
[2]University of Bristol, Department of Earth Sciences, Bristol, U. K. E-mail: james.verdon@bristol.ac.uk; gljmk@bristol.ac.uk.

derive a 1D empirical formulation to link vertical traveltime perturbations to changes in vertical strain and velocity from time-lapse seismic data. Prioul et al. (2004) apply third-order elasticity (TOE) theory to develop an empirical nonlinear rock-physics model capable of describing stress-dependent elasticity and anisotropy. Bakulin et al. (2000), Shapiro (2003), and Shapiro and Kaselow (2005) provide nonlinear formulations derived from first principals that are consistent with various empirically derived phenomenological equations (e.g., Zimmerman et al., 1986).

Only recently have nonlinear rock physics models been applied to coupled fluid-flow and geomechanical simulations to predict seismic attributes (e.g., Olden et al., 2001). Herwanger and Horne (2005) apply the empirical model of Prioul et al. (2004) to coupled flow-geomechanical simulation results and predict seismic anisotropy related to reservoir-production stress perturbations. Angus et al. (2008) apply the analytic microstructural model of Verdon et al. (2008) to predict the influence of fault transmissibility on seismic velocities and stress-induced seismic anisotropy. However, in these studies, the stress-dependent behavior of the dynamic elasticity is based on a limited number of field/core data.

In this paper, we examine the input parameters of the analytical microstructural stress-dependent model of Verdon et al. (2008). The analytical formulation is an extension and adaptation of the works of Tod (2002), Sayers (2002), and Hall et al. (2008). This approach is similar to TOE theory, except that the data are fitted to an exponential curve rather than two linear regimes at low and high effective stresses. The model is formulated in terms of an effective medium of idealized penny-shaped microcracks with initial crack density and initial aspect ratio. It can be applied to predict stress-induced elastic anisotropy as well as nonlinear and nonhysteretic elasticity.

Specifically, we explore crack properties of the analytical microstructural rock-physics model using laboratory measurements of ultrasonic velocities versus stress of dry core samples. We examine trends for various sedimentary rock lithologies to constrain the initial input parameters of the microstructural rock-physics model. We also explore the ratio of crack normal to tangential compliance and how this parameter affects our estimates of initial input parameters of the microstructural model. Establishing appropriate ranges of initial input parameters is essential for constructing dynamic elastic models from coupled fluid-flow and geomechanical simulation models.

ROCK-PHYSICS MODEL

Theoretical background

Sayers and Kachanov (1995) model the influence of stress-dependent elasticity resulting from microcrack deformation using the excess compliance approach of Schoenberg and Sayers (1995). Elastic anisotropy and stress dependence are expressed in terms of an excess compliance, given by

$$\Delta S_{ijkl} = \frac{1}{4}(\delta_{ik}\alpha_{jl} + \delta_{jk}\alpha_{il} + \delta_{il}\alpha_{jk} + \delta_{jl}\alpha_{ik}) + \beta_{ijkl}, \tag{1}$$

where δ_{ij} is the Kronecker delta. (Note that summation convention is used for equations 1–4.) The second- and fourth-rank crack-density tensors α_{ij} and β_{ijkl} are expressed

$$\alpha_{ij} = \frac{1}{V}\sum_m B_T^m n_i^m n_j^m S^m, \tag{2}$$

$$\beta_{ijkl} = \frac{1}{V}\sum_m (B_N^m - B_T^m) n_i^m n_j^m n_k^m n_l^m S^m. \tag{3}$$

Here, V is volume and B_N^m and B_T^m are the normal and tangential compliances across a microcrack (i.e., discontinuity surface), m having unit normal $\mathbf{n}$ and surface area S^m. Thus, the effective compliance S_{ijkl} of a rock can be expressed as

$$S_{ijkl} = S^0_{ijkl} + \Delta S_{ijkl}, \tag{4}$$

where S^0_{ijkl} is the background (or intact) rock compliance estimated from the mineral composition (Kendall et al., 2007) or behavior at high effective stresses (Sayers, 2002).

The main assumptions in deriving these expressions are that the microcracks be rotationally invariant and thin. Although equations 1–4 describe the excess compliance of cracks (e.g., Sayers, 2002; MacBeth, 2004; Hall et al., 2008), we seek an analytical formulation based on physically intuitive input parameters to forward model the nonlinear stress dependence of elasticity (and, hence, seismic velocities) resulting from the presence of cracks.

Analytical nonlinear model

To construct dynamic elastic models from coupled fluid-flow/geomechanical models, we require an analytical rock-physics model that can be calibrated using core data and has minimal initial input parameters. Verdon et al. (2008) apply the analytical effective-medium formulation of Tod (2002) to predict the anisotropic and stress-dependent seismic velocities presented in Hall et al. (2008). This analytical model is formulated in terms of a stress-dependent, second-rank crack-density tensor and crack aspect ratio to predict elastic anisotropy and stress dependence. The crack number density (hereafter referred to as crack density) is expressed as

$$\epsilon_i(\sigma^e_{ii}) = \epsilon_i^0 \exp[-c_i^r \sigma^e_{ii}], \tag{5}$$

where

$$c_i^r = \frac{1}{\pi \mu_i a_i^0}\left(\frac{\lambda_i + 2\mu_i}{\lambda_i + \mu_i}\right) \tag{6}$$

and where λ_i and μ_i are the Lamè constants, σ^e_{ii} is the principal effective stress in the ith direction, ϵ_i^0 is the effective initial crack density, and a_i^0 is the effective initial aspect ratio. (Hereafter, we do not use the term "effective" to describe initial crack density and initial aspect ratio. Later, we explain why "effective" is introduced for these initial model parameters.)

The second-rank microcrack density term is

$$\alpha_{ii} = \frac{\epsilon_i}{h_i}, \tag{7}$$

where $h_i = (3E_i^0[2 - \nu_i^0]/32[1 - (\nu_i^0)^2])$ is a normalization factor (Schubnel and Guéguen, 2003) and where E_i^0 and ν_i^0 are the anisotropic intact rock Young's modulus and Poisson's ratio. (Summation convention is not implied for equations 5–7.)

This derivation yields an expression for the effective elasticity that can model stress-induced anisotropy and nonlinearity from deviatoric stress fields. However, the derivation does not model the be-

havior of rock undergoing plastic or brittle deformation. Assuming penny-shaped cracks, where $\beta_{ijkl} = 0$ (see next section), and incorporating equation 7 into equation 1, the effective compliance predicted by the analytic rock-physics model is given by equation 4.

The necessary input parameters for the microstructural stress-dependent dynamic elasticity model are the background stiffness ($S^0_{ijkl} = 1/C^0_{ijkl}$), triaxial effective stress tensor σ_{ij}, initial crack density ϵ^0_i, and aspect ratio a^0_i. Coupled flow-geomechanical simulations supply the effective stress tensor, background stiffness, and density; therefore, the microstructural rock-physics model can be incorporated with the coupled flow-geomechanical simulation to construct dynamic elastic (i.e., seismic) models for seismic modeling applications. However, the initial crack density and aspect ratio remain poorly constrained.

Verdon et al. (2008) estimate the initial crack density and aspect ratio of several sandstone samples from the Clair reservoir (Kendall et al., 2007) and several thermally damaged sandstone samples (MacBeth and Schuett, 2007). The inversion results show initial crack densities ranging between approximately $\epsilon^0 \in (0.08,0.8)$ and initial aspect ratios ranging between $a^0 \in (0.0005,0.005)$. The inversion results for the thermal-damage experiment of MacBeth and Schuett (2007) confirm the expected result that initial crack density is sensitive to core damage.

Although instructive qualitatively, the range of values obtained from a limited number of sandstone samples is not compelling statistically. This is especially important if the nonlinear rock-physics model is to be linked with coupled flow-geomechanical simulation to predict the seismic response of a producing reservoir. Thus, it is necessary to improve constraints on the range of acceptable initial crack densities and aspect ratios from more core samples as well as various lithologies.

ROCK-PHYSICS MODEL CALIBRATION

Sayers (2002) and Hall et al. (2008) apply equations 1–4 to invert for the nonlinear elasticity tensor. In both studies, they find that reasonably accurate estimates of stress-dependent velocities can be obtained using only the second-rank crack-density term α_{ij}. Hall et al. (2008) further invert for the fourth-rank density term β_{ijkl} but assuming that β_{ijkl} is small and the result solely of the misfit between the data and the second-rank term α_{ij}. Verdon et al. (2008) also perform a joint inversion for α_{ij} and β_{ijkl} without assuming a priori that β_{ijkl} is small. The results from Hall et al. (2008) and Verdon et al. (2008), using a limited data set, suggest that the magnitude of β_{ijkl} is such that the scalar crack assumption (see following discussion) is a reasonable approximation.

To constrain the input parameters of the analytical microstructural rock-physics model, we apply the approach of Verdon et al. (2008) to evaluate the excess compliance of stress versus ultrasonic velocity measurements of dry core samples. First, we perform a scalar crack inversion, where we invert only for the second-rank crack-density term (equation 2) and assume the fourth-rank term (equation 3) is negligible ($\beta_{ijkl} = 0$). Second, we perform the joint inversion, where we invert for the second- and fourth-rank crack-density terms. We subsequently use the inverted second-rank density term to solve for the best-fitting initial crack density ϵ^0 and initial aspect ratio a^0 via equations 5–7.

To summarize, the scalar crack and joint inversions assume only that the microcracks are rotationally invariant and thin. However, when solving for the best-fitting initial crack density and aspect ratio, we also assume that the microcracks are penny shaped to introduce a measure of crack aspect ratio. Figure 1 describes the workflow to evaluate the best-fitting input parameters ϵ^0 and a^0 of the analytical microstructural model.

Significance of β_{ijkl}

Before discussing the results of the inversions, it is useful to consider the significance of the fourth-rank crack-density term. For most rocks, the fourth-rank term β_{ijkl} is often assumed negligible, and only the contribution from the second-rank term α_{ij} is thought sufficient in describing the nonlinear stress-dependent elasticity (Grechka and Kachanov, 2006; Hall et al., 2008; Verdon et al., 2008). For small values of β_{ijkl} and assuming penny-shaped cracks, the ratio of crack normal to tangential compliance B_N/B_T is approximately one. The so-called scalar crack assumption refers to the special case when $B_N/B_T = 1$. With the scalar crack assumption, the excess compliance resulting from a distribution of penny-shaped displacement discontinuities can be assessed by considering only contributions of the three diagonal components of α_{ij}. Thus, α_{ij} can be used to describe the orientation and density of three mutually orthogonal sets of aligned microcracks.

For example, Sayers and Kachanov (1995) note that for Berea Sandstone, the Poisson's ratio ν is 0.1–0.2; for such a case, using only α_{ij} can yield a reasonable approximation of the rock-stress sensitivity. This is because when ν is small, β_{ijkl} is an order of magnitude smaller than α_{ij}. However, ν for sedimentary rocks is typically 0.1–0.4. Thus, for larger values of Poisson's ratio, the assumption of penny-shaped and scalar cracks may not be the most appropriate for estimating the behavior of all reservoir rocks.

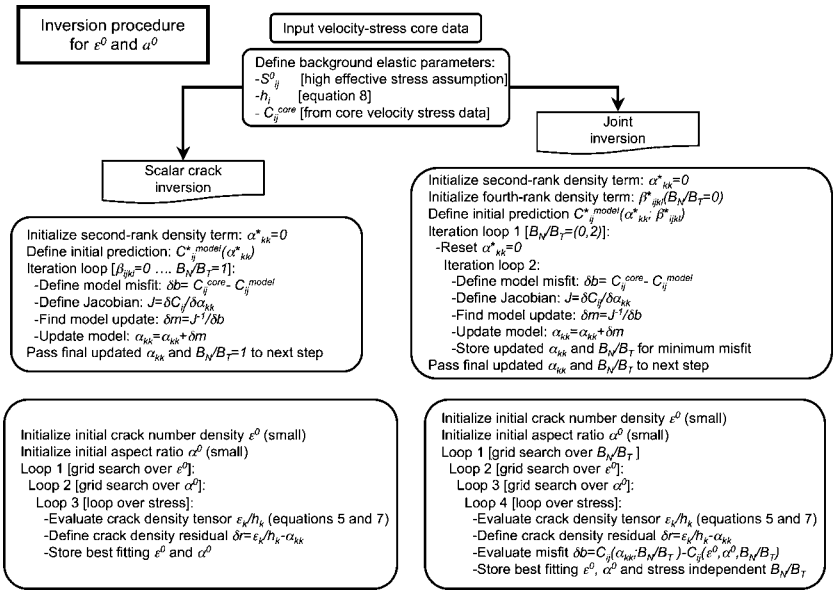

Figure 1. Flowchart highlighting the inversion procedure for the scalar crack and joint inversions.

Various mathematical expressions exist for representing the ratio of normal-to-tangential compliance of a discontinuity surface (e.g., crack), such as

$$\frac{B_N}{B_T} = \left(1 - \frac{\nu}{2}\right) \text{ and } \frac{B_N}{B_T} = \left(\frac{1-\nu}{1-\frac{\nu}{2}}\right) \quad (8)$$

for a planar distribution of drained small, isolated cracks and drained rough surfaces (Lubbe et al., 2008), respectively. For $\nu \in (0.1,0.4)$, one would predict the range of B_N/B_T for dry (or gas-filled) discontinuities to be (0.75,0.95). However, laboratory estimates of B_N/B_T for sandstone (MacBeth and Schuett, 2007) and limestone (Lubbe et al., 2007, 2008) dry core samples have found values significantly lower than unity, with ratios of 0.0-0.6. MacBeth and Schuett (2007) also note that for (thermally) damaged samples, the ratio may increase to values above unity. Deviations from the scalar crack assumption potentially result from several factors, such as the presence of fluids with nonzero bulk modulus, cement or clay within cracks, and more complex crack geometries (i.e., nonidealized penny-shaped cracks). Later, we show that B_N/B_T for sedimentary rocks is, on average, less than unity and that the scalar crack assumption generally is invalid.

Table 1. Published stress core data for various lithologies.

Lithology	Study
Sandstone	King (1966, 2002), Rojas (2005), He (2006), Hemsing (2007), MacBeth and Schuett (2007), Grochau and Gurevich (2008), Hall et al. (2008)
Tight-gas sandstone	Jizba (1991)
Shale	Johnston and Christensen (1995), Hemsing (2007)
Tight-gas shale	Jizba (1991)
Limestone	Simmons and Brace (1965), Nur and Simmons (1969), Brown (2002)
Dolostone	Nur and Simmons (1969), Brown (2002)
Conglomerate	He (2006)
Carbonates/anhydrites	Hemsing (2007)

RESULTS

In this section, we apply our approach to more than 150 ultrasonic velocity versus stress dry core measurements from various studies (Table 1). The results are examined for any lithologic and depth dependence of ϵ^0 and a^0, which may provide important initial constraints. Results from the joint inversion are used to examine the significance of β_{ijkl} on evaluating ϵ^0 and a^0 as well as to explore the range of estimated B_N/B_T. Finally, we examine the errors introduced in estimating the initial input parameters ϵ^0 and a^0 of the analytic microstructural rock-physics model by inverting for only α_{ij} when $B_N/B_T \neq 1$ using synthetically generated data.

In compiling the data, we convert all velocity measurements into an elastic tensor, where the symmetry of the elastic tensor is determined by the number of directionally independent P- and S-wave measurements available. When only one P- and one S-wave velocity are available, the elastic tensor is assumed isotropic. Because most of the results are isotropic (i.e., generally only one P- and one S-wave measurement available), all anisotropic elastic tensors are converted to an isotropic equivalent tensor to allow global comparison of all inversion results. Evaluation of the isotropic equivalent of an anisotropic elastic tensor is performed using a Voigt-Reuss-Hill directional averaging approach (Kendall et al., 2007). However, our rock-physics model is not restricted to isotropy. Not only can the background elasticity (or compliance) be anisotropic, but directionally dependent velocity measurements also can be used to evaluate anisotropy in ϵ^0 and a^0.

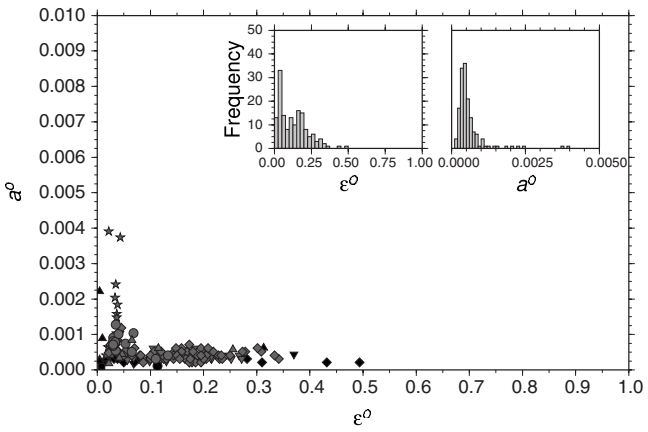

Figure 2. Comparison of initial crack density ϵ^0 versus initial aspect ratio a^0 for dry core samples for all lithologies after inverting for α_{ij} only: anhydrite (black square), carbonate (black inverted triangle), conglomerate (black diamond), dolostone (black circle), limestone (black triangle), sandstone (gray inverted triangle), shale (gray star), tight-gas sandstone (gray diamond), tight-gas shale (gray circle), and Clair Sandstone (gray triangle). Inset (also Figures 3, 5, and 6) are histograms for ϵ^0 and a^0.

Scalar crack inversion (α_{ij} only)

Figure 2 displays ϵ^0 versus a^0 estimates from the scalar crack inversion procedure for all of the dry core samples. Also shown (inset) are histograms for ϵ^0 and a^0. The initial aspect ratios show some scatter, but there is a remarkable clustering with a mean of approximately $\bar{a}^0 = 0.0004$. This result is consistent with the aspect-ratio inversion of King (2002) for a Crosland Hill Sandstone sample (the effective medium model consists of sets of aligned oblate spheroidal discontinuities with transversely isotropic symmetry). The initial-crack-density estimates in Figure 2 show much more scatter, falling between $\epsilon^0 \in (0.0,0.5)$ and having a mean $\bar{\epsilon}^0 = 0.1$. There appears to be no systematic trend for lithology, except that the shale and limestone samples have initial aspect ratios ranging between approximately $a^0 \in (0.001,0.004)$, greater than the global trend of the dry samples.

Table 2 summarizes the mean estimates for various lithologies for ϵ^0 and a^0. The initial aspect ratio of shale differs significantly from the other lithologies — approximately twice in magnitude. The sandstone and tight-gas sandstone lithologies have initial crack densities of approximately 0.15, whereas the shales and carbonates have values of 0.04 and 0.08, respectively.

We also examine ϵ^0 and a^0 with depth and porosity but notice no observable trends. However, most of the core samples are taken from surface outcrops or reservoir depths. Thus, the limited depth distribution in the data is insufficient to extract any depth and porosity trends in ϵ^0 and a^0.

Although shales are very abundant in reservoir systems, relatively little is known about their geomechanical properties, primarily because of their fine grain size and, until recently, lack of interest from hydrocarbon production programs. Shales represent a broad class of siliciclastic rocks and generally encompass any rock with greater than 50% clay content. Because shales behave mechanically quite differently from sandstones, it is instructive to examine the inversion results in terms of individual lithologies.

In Figure 3, ϵ^0 versus a^0 is plotted for two separate lithologies: sandstones and clay-rich samples. The insets are histograms for ϵ^0 and a^0. For the sandstone samples (Figure 3a), initial-aspect-ratio estimates cluster tightly around 0.0004, with significant variation in initial crack density ranging between 0 and 0.5. In Figure 3b, a^0 shows significant scatter and ϵ^0 less scatter for the clay-rich samples. For the pure shale samples, only three fall within the range of the initial-aspect-ratio global average; the Mannville Shale core samples provided by Hemsing (2007). The Mannville Shales consist largely of quartz with a significant amount of clay content. However, the clay content within these three samples is on the lower end of typical shales (Hemsing, 2007), which may explain why the estimated initial aspect ratios for these shaly sandstones are similar to those of the global trend (i.e., sandstones). The tight-gas shale samples (from Jizba, 1991) also display initial-aspect-ratio estimates sensitive to clay content consistent with the pure shale samples. Figure 3b shows the Clair Sandstone estimates (gray triangles B–F and I) for comparison.

Clair Sandstone samples

One issue with analyzing data compiled from various published sources is that experimental procedure and equipment can vary significantly from study to study as well as over time. Furthermore, the core-sample observations provided can be limited (e.g., only density, porosity, velocities, and effective stresses). Access to detailed core-sample description can provide valuable information to complement ultrasonic velocity measurements, which often are unavailable in published studies. Thus, we are limited to general conclusions based on global trends.

Measurements of the reservoir sandstone core samples from the Clair field obtained during the Seismic Anisotropy as an Indicator of Lithology (SAIL) consortium project (see Kendall et al., 2007) represent a subset of the compiled data that provide additional core physical properties. For each of these samples, there are detailed petrophysical analysis, such as quantitative X-ray diffraction for mineralogical analysis of the mineral constituents; electron backscattered diffraction (EBSD) to characterize the orientation of quartz, feldspar, and calcite grains; and X-ray texture goniometry and image analysis to evaluate crystal preferred orientation (CPO) of mica and clay grains.

Table 3 shows various sample physical properties for the six Clair Sandstone samples and the estimated ϵ^0 and a^0 (see labeled gray triangles in Figure 3). Samples E, F, and I represent clean sandstone and show initial aspect ratios consistent with the general trend of all of the sandstone samples but with significant variation in initial crack densities. Sample E has been chemically cleaned and may be more representative of a damaged sample. Samples B, C, and D have increasing clay content (approximately 12%, 35%, and 30%, respectively) but still show initial aspect ratios consistent with the general trend of all sandstones. However, sample C has the highest clay content and displays the greatest initial aspect ratio.

It is difficult to conclude with any certainty from the Clair Sandstones alone that increased clay content leads to increased initial aspect ratio. Interpretation of the behavior of the Clair Sandstones might be affected by the fact that Clair field has undergone significant uplift during its geologic evolution. Furthermore, the stress-velocity data for these samples deviate to varying degrees from the typ-

Table 2. Summary of $\bar{\epsilon}^0$ and $\bar{a}^0$ estimated for each lithology after inverting for α_{ij} only.

Parameter	All lithologies	Sandstones	Shales	Carbonates	Tight-gas sandstones
$\bar{\epsilon}^0$	0.1200	0.1550	0.0350	0.0829	0.1500
$\bar{a}^0$	0.0004	0.0004	0.0008	0.0005	0.0004

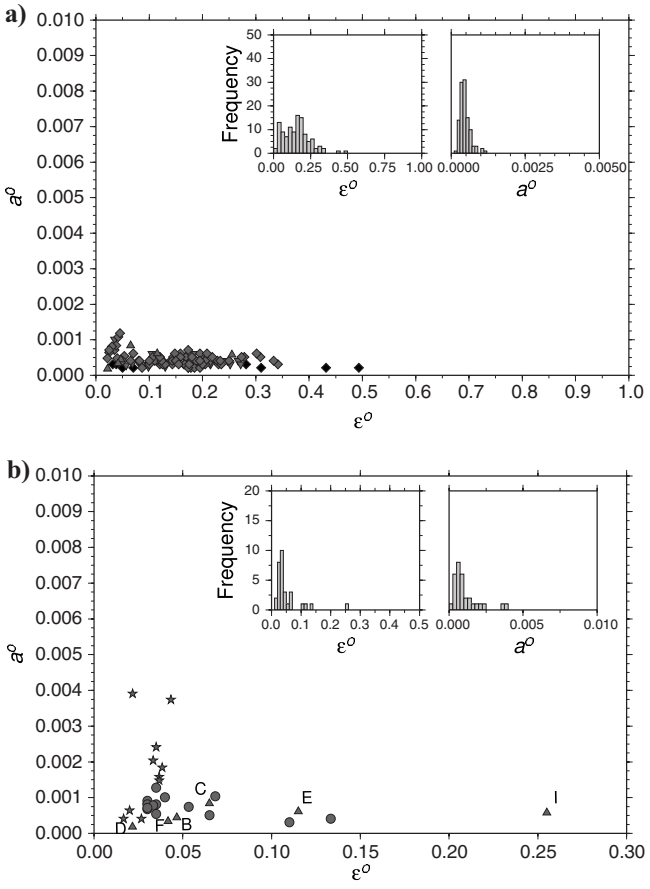

Figure 3. Comparison of ϵ^0 versus a^0 for (a) dry sandstone and (b) shale-rich cores after inverting for α_{ij} only (see Figure 2 for symbol legend). The Clair Sandstones are labeled B–F and I (see Table 3 for petrophysical details).

ical exponential stress sensitivity with increasing pressure typical of most sedimentary rocks. However, the results from the shale samples as well as the Clair Sandstones suggest a relation between clay and mica content and initial aspect ratio. More velocity-stress data for shales and shaly (clay-rich) sandstones, with accompanying petrophysical analyses, are necessary to study the potential link between shale content and increasing aspect ratio.

To understand how mica and clay might influence estimates of the initial aspect ratio, it is helpful to examine the microstructure of the clean and shaly sandstones. In Figure 4, EBSD images are shown for the clean sandstone samples F and I and the shaly sandstone sample C. The microstructure of the clean sandstone samples shows remarkable consistency in orientation of quartz and feldspar grains associated with paleoflow, whereas the calcite and dolomite grains show random orientation as a result of their diagenetic origin (Valcke et al., 2006). The EBSD image of shaly sample C shows a CPO of the mica-clay grains with vertical symmetry resulting from mechanical compaction. The orientation of the quartz and feldspar grains is similar to the clean samples.

Comparing the microstructural images of the clean sandstones with the shaly sandstone highlights the dominance of the mica and clay grains. The dominance of the clay-rich minerals is also observed in the seismic anisotropy analysis of Kendall et al. (2007), where the presence of 20–40% combined mica and clay grains leads to a dominant vertically transversely isotropic (VTI) signature. However, it is unclear how much this strong lithologic anisotropy influences the initial-aspect-ratio estimates. For example, does this initial VTI skew the inversion estimates of initial aspect ratios, or does the presence of significant amounts of mica and clay grains lead to an inherent microstructural bias of physically larger microcrack aspect ratio? Further study is necessary.

Full inversion (α_{ij} and β_{ijkl})

Figure 5 shows the results of the more than 150 ϵ^0 versus a^0 estimates using the joint inversion procedure. Also shown (inset) are the histograms for ϵ^0 and a^0. The general trend within this figure is comparable to that of Figure 2. The behavior of a^0 appears similar but with the few outlying data points falling much farther away from the general trend. In terms of initial crack density, the scatter increases, as seen in the broader distribution in the inset histogram.

Table 4 summarizes the mean estimates for various lithologies for ϵ^0 and a^0. The initial aspect ratio of shale again differs significantly from the other lithologies, being approximately twice in magnitude. Also, the inversion for a^0 seems to be insensitive to the magnitude of β_{ijkl}, suggesting that inverting for only α_{ij} can yield consistent estimates of initial aspect ratio. The sandstone, tight-gas sandstone, and carbonate lithologies all have similar orders-of-magnitude initial crack densities of approximately 0.12–0.14, whereas the shale lithology has a value of 0.02. Interestingly, the misfit between observed and predicted elasticity improves with the joint inversion. This is expected because including the fourth-rank tensor within the inversion allows the influence of crack normal compliance to be modeled. In general, this suggests that the results from the joint inversion should provide a more reliable description of the microcrack characteristics than the scalar crack inversion.

In Figure 6, initial crack density versus aspect ratio are plotted for sandstones and clay-rich samples. Inset within both are histograms for ϵ^0 and a^0. For the sandstone samples (Figure 6a), initial-aspect-ratio estimates cluster tightly around 0.0004, with significant variation in initial crack density (0–0.9). For the clay-rich samples (Figure 6b), a^0 shows slightly more scatter, whereas the distribution is less diffuse for ϵ^0. For the pure shale samples, no samples fall within the range of the initial-aspect-ratio global average. However, the shale core samples as well as the tight-gas shale samples still display initial-aspect-ratio estimates sensitive to clay content.

Also shown in Figure 6b are the Clair Sandstone ϵ^0 and a^0 estimates (triangles B–F and I), where the percent clay content is known quantitatively for each sample. The clean sandstone samples B, F, and I have initial aspect ratios consistent with the sandstone lithology trend. The clay-rich samples C and D as well as the chemically cleaned sandstone sample E have initial aspect ratios larger than the

Table 3. Rock properties of Clair Sandstone samples with percentage of modal constituents and mean estimated initial crack density and initial aspect ratio for inversions using α_{ij} only (top) and α_{ij} and β_{ijkl} (bottom). Adapted from Maddock (2006; his Table C.1).

Sample	Depth (m)	Porosity (%)	Permeability (mD)	Quartz (%)	Feldspars (%)	Calcium/ Dolomite (%)	Phyllo-silicates (%)	$\bar{\epsilon}^0$	$\bar{a}^0$
B	1784	12.0	24.00	38.64	18.26	18.26	12.85	0.0467	0.0004
								0.3983	0.0001
C	1788	8.0	0.02	30.89	25.41	1.32	34.38	0.0650	0.0008
								0.1333	0.0008
D	1841	11.0	0.07	30.97	21.77	5.92	30.24	0.0217	0.0002
								0.0083	0.0099
E	1909	13.0	2.80	54.95	16.07	10.48	5.51	0.1150	0.0006
								0.0833	0.0014
F	1950	14.8	84.00	44.19	30.46	7.45	3.10	0.0417	0.0003
								0.0433	0.0003
I	2194	12.1	1.40	61.05	12.62	8.06	6.18	0.2550	0.0006
								0.1450	0.0005

sandstone average. For these samples, joint inversion for α_{ij} and β_{ijkl} only marginally improved the misfit between observed and predicted elasticity.

Estimating B_N/B_T

The joint inversion procedure for α_{ij} and β_{ijkl} developed by Verdon et al. (2008) is formulated on the assumption that the microcracks are thin and shaped identically (i.e., rotationally invariant) and that β_{ijkl} is isotropic to simplify the set of equations used in the inversion procedure. With these assumptions, the fourth-rank tensor can be expressed in terms of the second-rank tensor:

$$\beta_{1111} = \beta_{2222} = \beta_{3333} = \frac{1}{3}\left(\frac{B_N}{B_T} - 1\right)\alpha^m, \tag{9}$$

$$\beta_{1122} = \beta_{1133} = \beta_{2233} = \beta_{1212} = \beta_{1313} = \beta_{2323} = \frac{1}{3}\beta_{1111}, \tag{10}$$

where

$$\alpha^m = \text{trace}(\alpha_{ii}) \text{ and } \alpha_{ii} = \frac{\pi N r^2}{3V} B_T \tag{11}$$

(Sayers and Han, 2002). The scalar N is the number of discontinuities in a volume V, and r is the radius of the crack. Similar to Verdon et al. (2008), we perform a grid search over B_N/B_T, with a range of allowable values between $B_N/B_T \in (0.0,2.0)$.

In Figure 7, histograms for B_N/B_T are shown for all lithologies as well as for the sandstone and carbonate samples. For all lithologies (Figure 7, shaded), the estimate ratios span the entire range, with most falling within approximately 0.4–1.5. The inversion for B_N/B_T is unstable at high confining stresses, so we disregard estimates at these stresses. The instability arises because we estimate the background compliance S^0_{ijkl} in equation 4 using the high-stress-compliance approach of Sayers (2002) (there is no information on mineral compliance for most of the core data with which to estimate S^0_{ijkl}). As a result, when the effective stress approaches the highest stress, S^0_{ijkl} approaches the high stress compliance and leads to instability in the inversion procedure. Ratio estimates below 0.25 and above 1.75 are predominantly a result of poor data or deviations from isotropic β_{ijkl}. The sandstone samples (Figure 7, blue line) are characterized by B_N/B_T between 0.25 and 1.0, with a significant frequency around 0.6. The carbonate samples (Figure 7, red line) show similar characteristics but with a slightly skewed distribution and peak around 0.55.

Figure 8 compares the B_N/B_T estimates for the sandstone (shaded) and tight-gas sandstone lithologies. For all the tight-gas sandstones of Jizba (1991) (Figure 8, blue line), the distribution is much broader and skewed to higher ratios, with a weak peak around 0.75 and significant frequencies up to 1.75. Focusing on the results from Rojas (2005) (Figure 8, red line), the tight-gas samples have values of 0.25–1.25 and have B_N/B_T characteristics similar to those of the sandstone lithologies. However, those from Jizba (1991) differ significantly; possible reasons for this may be that the specific samples are cemented poorly or may have been damaged during core extraction and/or reservoir production (e.g., hydraulically induced fracturing).

Figure 9 shows the results for B_N/B_T estimates for the shale and tight-gas shale lithologies. The distribution of all shale samples (Figure 9, shaded) and the shale samples of Hemsing (2007) (Figure 9, red line) fall mainly within 0.0–1.5. The results for the tight-gas shales (Jizba, 1991) (Figure 9, blue line) are just as diffuse, with

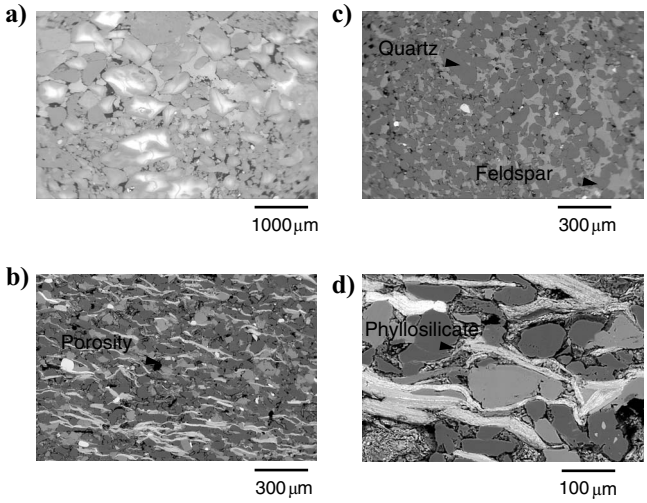

Figure 4. Back-scatter electron images of Clair Sandstone samples: clean sandstone samples (a) F and (c) I, and (b, d) clay-rich sandstone sample C (from Maddock, 2006).

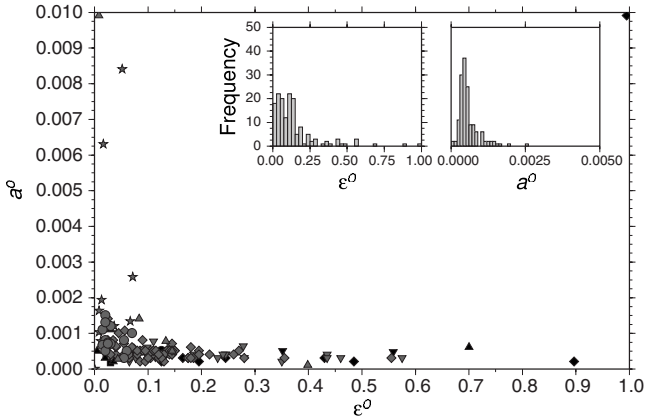

Figure 5. Comparison of ϵ^0 versus a^0 for dry core samples for all lithologies after inverting for α_{ij} and β_{ijkl} (see Figure 2 for symbol legend).

Table 4. Summary of $\bar{\epsilon}^0$ and $\bar{a}^0$ estimated for each lithology after inverting for α_{ij} and β_{ijkl}.

Parameter	All lithologies	Sandstones	Shales	Carbonates	Tight-gas sandstones
$\bar{\epsilon}^0$	0.1100	0.1300	0.0200	0.1394	0.1100
$\bar{a}^0$	0.0004	0.0004	0.0010	0.0005	0.0004

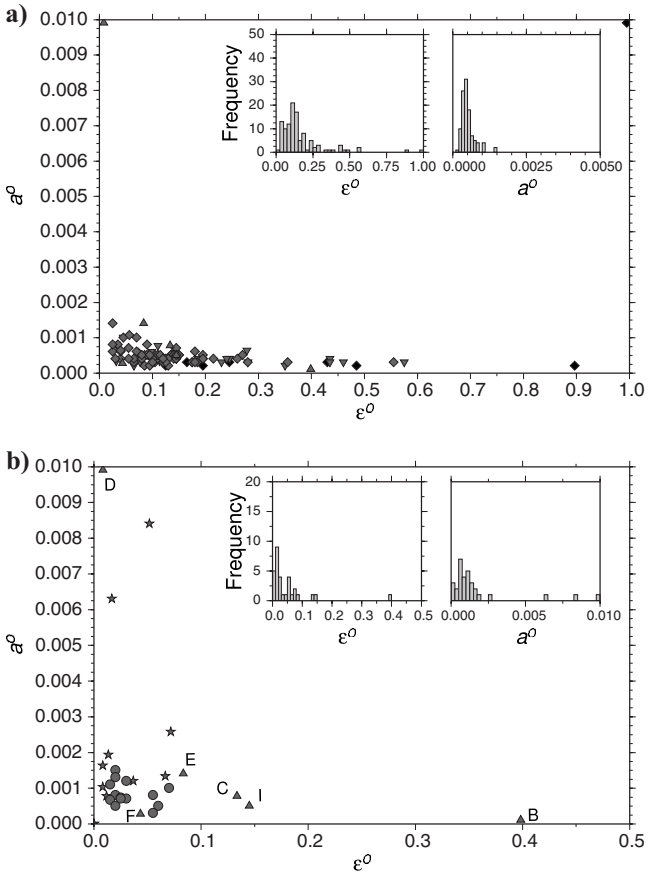

Figure 6. Comparison of ϵ^0 versus a^0 for (a) dry sandstone cores and (b) shale-rich cores after inverting for α_{ij} and β_{ijkl} (see Figure 2 for symbol legend).

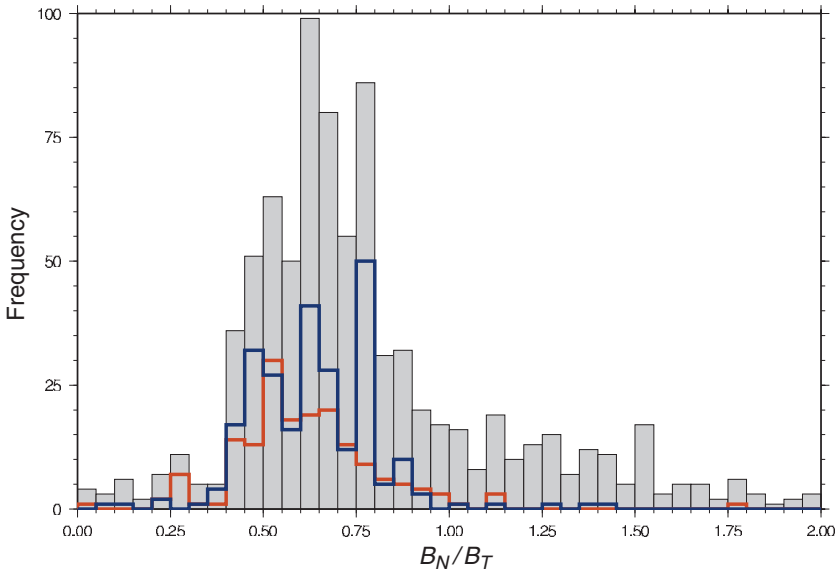

Figure 7. Frequency histograms of inverted B_N/B_T for all lithologies (gray shaded), sandstone samples (blue outline), and carbonate samples (red outline).

clusters of 0.6–1.5. However, there are relatively limited data for the shales, so it is difficult to draw any definitive conclusions other than that the range of B_N/B_T can vary between 0.0 and 1.75.

For comparison, we estimate B_N/B_T using the velocity-stress data for the aeolian Rotliegend Sandstone samples presented in MacBeth and Schuett (2007; their Figures 3, 4, and 6). The results for the undamaged samples (Figure 10, shaded) show a distribution of 0.0–0.8 with a mean of approximately 0.6. For the thermally damaged samples (Figure 10, red line), we also observe an increase in the range of B_N/B_T, with values of 0.0–1.9. These results show some similarity with those of MacBeth and Schuett (2007, their Figure 7c), except that our estimated means are significantly larger. Potential sources of discrepancy between our results and theirs are theoretical differences in methodology, errors introduced from digitizing the graphical data into discrete velocity versus stress data, and applying the high stress assumption to estimate background elasticity.

Errors introduced by inverting for α_{ij} only

The results from the previous section clearly demonstrate that the scalar crack assumption is inconsistent with the joint inversion results of the velocity-stress core data. This stresses the importance of inverting for the second- and fourth-rank crack-density terms to predict nonlinear elasticity more accurately, at least in terms of the initial crack density and initial aspect ratio. The question that arises is the effect that neglecting the fourth-rank tensor has on estimates of initial crack density and initial aspect ratio for the nonlinear analytic rock-physics model of Tod (2002). In this section, we perform a numerical test to examine the inversion results for the scalar crack assumption as well as for α_{ij} and β_{ijkl}.

A synthetic stress versus velocity data set is generated using a representative sedimentary anisotropic mineral elasticity (Raymer et al., 2000) as the background elasticity. The stress dependence is evaluated using equations 1–4 (see Sayers, 2002; Hall et al., 2008; Verdon et al., 2008), where α_{ij} is determined by equation 7 and β_{ijkl} is determined using relations 9 and 10. A total of 84 synthetic core experiments are generated for a range of $B_N/B_T \in (0.0,2.0)$ at increments of 0.1 for four sets of initial crack density and initial aspect ratio: $(\epsilon^0,a^0) = (0.1,0.0005)$, (0.5, 0.0005), (0.1, 0.001), and (0.5, 0.001). For the inversion procedure, we use the high-stress assumption to approximate the mineral elasticity for the scalar crack and joint inversions.

Figure 11 shows the absolute errors of the scalar crack and joint inversions for the synthetic data set. For the initial-crack-density estimates (Figure 11a), the joint inversions yield essentially identical estimates. This is to be expected because the only difference between the synthetic data and the estimated data is that the estimated data use the high stress compliance of the synthetic data as an estimate of the background elasticity and not the true mineral compliance. There is significant error for the scalar crack inversion, where accurate estimates are obtained only for inversions where synthetic data have B_N/B_T close to unity. For low B_N/B_T, ϵ^0 is underestimated, whereas it is overestimated for high B_N/B_T. This has important implications in estimating and pre-

dicting rock damage (i.e., induced fracturing) in terms of crack-density estimates. For the initial aspect ratio (Figure 11b), the joint inversion yields accurate inversions as expected. Although the scalar crack inversion produces accurate results for B_N/B_T between 0.7 and 1.6, it becomes less reliable for values below 0.4.

These results suggest that it is important to evaluate the second- and fourth-rank tensors to estimate properly the initial parameters of the nonlinear rock-physics model of Tod (2002). The results also indicate that a correction term may be necessary for this analytical model if the influence of the crack compliance ratio is significant. A first-order approach would be to introduce a stress-independent fourth-rank term based on an average B_N/B_T ratio estimated from the core data. Thus, the stress-dependent elasticity tensor can be constructed using the crack-density terms 7 and equations 1–4 and 9–11.

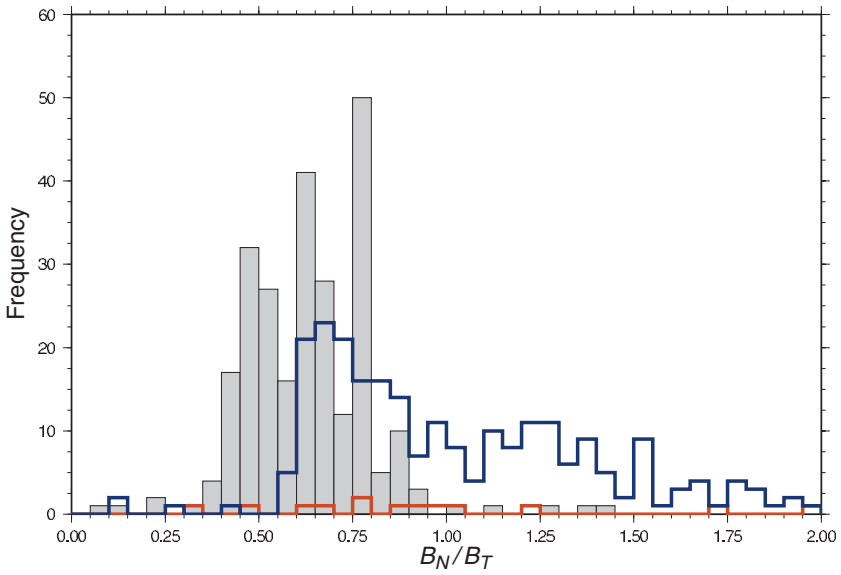

Figure 8. Frequency histograms for inverted B_N/B_T for sandstone and tight-gas sandstone lithologies: sandstone samples (gray shaded), tight-gas samples from Rojas (2005) (red outline), and tight-gas samples from Jizba (1991) (blue outline).

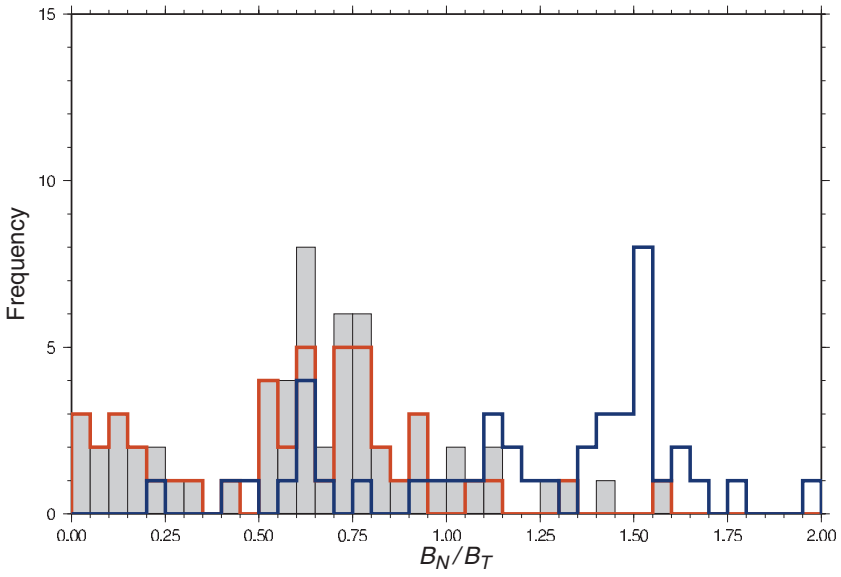

Figure 9. Frequency histograms for inverted B_N/B_T for shale lithologies: all shale samples (gray shaded), Hemsing (2007) shale samples (red), and Jizba (1991) tight-gas shale samples (blue).

DISCUSSION

Although the microstructural nonlinear rock-physics model is not a rigorous description of the true microstructure of sedimentary rock, it does provide an accurate means of predicting the averaging effects of the microstructure in terms of wave properties. Furthermore, this effective medium model is very attractive conceptually because it is formulated in terms of two initial parameters: effective initial crack density ϵ^0 and effective initial aspect ratio a^0, which can be linked to rock microstructure. Referring to equations 5–7, increasing ϵ^0 results in a weaker or more compliant rock. Although a^0 does not affect the overall strength of the rock, it does influence stress sensitivity. For example, increasing a^0 leads to lower stress sensitivity of the elasticity at lower confining stresses.

The way these effective-medium parameters relate to real physical (mechanical) properties of the rock is not trivial. For real rock, an increase in crack density most likely is related to opening existing cracks, generating new grain boundaries, and/or breaking existing intergrain cement bonds. Thus, the effective crack density represents a proxy for damage on the grain scale. The effective a^0 is related to the shape of the nonequant porosity void space. Thus, for real rock, the effective a^0 describes the average shape (or more dominant shape distribution) of the stress-sensitive microcracks. Relating the effective medium estimate of B_N/B_T to the actual microcrack compliance behavior is more tenuous. However, the range of the estimated ratios (0.25–0.75, with a mean of approximately 0.55) is consistent with discontinuities modeled as rough surfaces in contact under confining stresses (Palciauskas, 1992; MacBeth and Schuett, 2007). The estimated ratios for damaged samples fall predominantly between 0.25 and 1.75, where the microcracks of the thermally damaged samples have clean linear geometry (MacBeth and Schuett, 2007). Because planar surfaces are expected to have higher normal compliance than imperfect surfaces (i.e., smooth planar surfaces have fewer asperities to resist closure), we expect that clean, planar microcracks will have higher B_N/B_T (MacBeth and Schuett, 2007). Furthermore, for fluid-filled discontinuities, B_N/B_T would be altered by the change in compressibility of the crack-filling material, where the ratios are predicted to be lower (e.g., Sayers and Han, 2002; Worthington, 2008).

The influence of clays and fluids within microcracks as well as capillary forces has important implications on the stress sensitivity of rocks (Van Den Abeele et al., 2002). However, more research is needed to establish the links between mechanical properties of rocks with respect to clay, fluids, and capillary forces. Specifically,

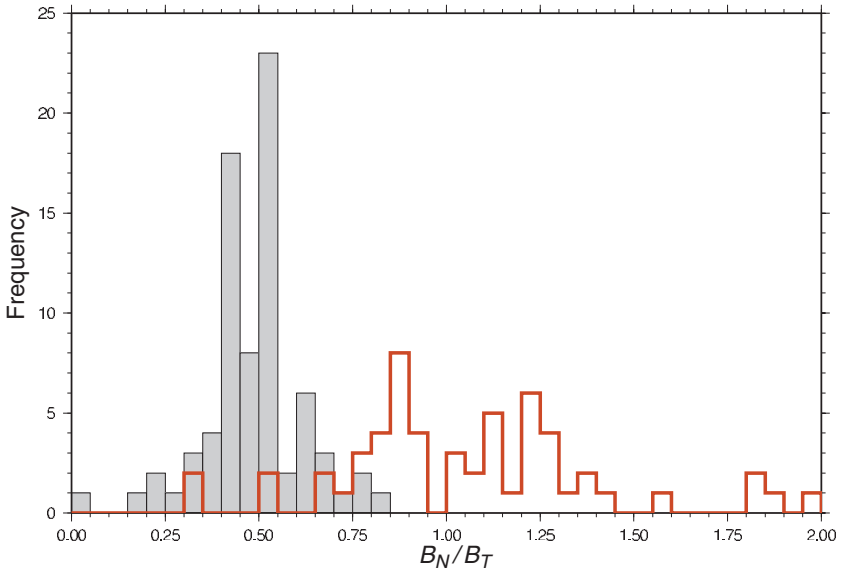

Figure 10. Frequency histograms of inverted B_N/B_T for undamaged (gray shaded) and damaged (red outline) Aeolian Rotliegend sandstone samples from MacBeth and Schuett (2007).

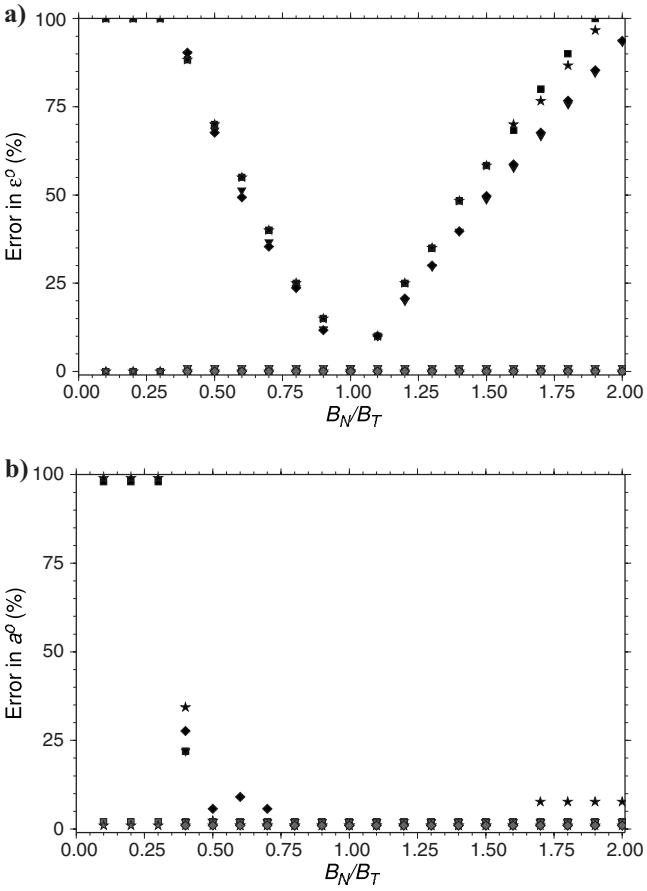

Figure 11. Comparison of absolute errors from inversion of synthetic data set for (a) ϵ^0 and (b) a^0 for scalar crack inversion (black symbols) and joint inversion (gray symbols). Symbols are for (ϵ^0,a^0) sets (0.1, 0.0005 — squares), (0.5, 0.0005 — inverted triangles), (0.1, 0.001 — stars), and (0.5, 0.001 — diamonds).

how do clay minerals, fluids, and capillary forces influence the microstructural rock-physics model parameters: initial aspect ratio, initial crack density, and B_N/B_T? Furthermore, the influence of fluids is particularly problematic in measuring elastic properties of so-called dry (or room-dry) shale and clay-rich core samples. This is because clay-rich rocks rarely are dried completely because of, for example, the presence of strong capillary forces. If the samples were completely dry, it is likely their microstructure and elastic properties would be changed irreversibly (Boris Gurevich, personal communication, 2009).

A key result of this study is the implication that estimating the second-rank crack-density term, assuming the fourth-rank tensor is negligible (i.e., the scalar crack assumption), can lead to large errors in estimating ϵ^0 when B_N/B_T deviates from unity. Specifically, full inversion for the second- and fourth-rank crack-density tensors is necessary to characterize the stress sensitivity of rock properly. This is particularly important if the inversion scheme is used to evaluate the input parameters for the nonlinear microstructural rock-physics model.

To apply crack density routinely as a proxy for damage, more analysis of core data is needed to quantify rock damage in terms of initial crack density. The ability to link damage to an effective crack-density parameter would allow us to explore quantitative assessment of induced fracturing using techniques such as shear-wave splitting analysis. From a qualitative perspective, initial aspect ratio can be used as a proxy for the stress sensitivity of rock. Although aspect ratio varies with lithology, it remains relatively well constrained for sandstones, tight-gas sandstones, and carbonates but varies significantly for shales. Understanding why initial aspect ratio is significantly different for shales and relatively consistent for all other lithologies may allow us to understand better how the mechanical properties of shales affect seismic waves.

Measurements of rock-physics properties of dry core samples provide valuable information on the elastic properties of sedimentary rocks. However, sedimentary rocks are seldom under dry conditions, so a more realistic characterization of rock-physics properties should be examined under fluid-saturated conditions (e.g., Han, 1986). It is expected that the dispersive effects of the fluid-filled cracks as well as viscosities of the saturating fluids can effect velocity measurements significantly at ultrasonic frequencies, so extension of the inversion procedure to include the effects of squirt flow will be necessary. By incorporating an effective squirt-flow model, we can explore the role that fluids may have on crack density, aspect ratio, and B_N/B_T.

CONCLUSION

We have inverted for the stress-sensitive microcrack parameters of more than 150 dry sedimentary core samples and have evaluated the results in terms of a microstructural nonlinear rock-physics model. From these results, the input parameters (initial crack density ϵ^0 and initial aspect ratio a^0) are constrained on the basis of lithology. For most sedimentary lithologies, a^0 clusters tightly around 0.0004, and for clay rich lithologies around 0.001. The results for ϵ^0 are more

diffuse and vary significantly between lithologies. This variation likely has more to do with core damage than lithological differences in the microstructure.

Estimates of the crack normal to tangential compliance B_N/B_T indicate that for intact and damaged rocks, the range of values is 0.0–2.0. The global trend suggests that B_N/B_T clusters around 0.6, which also is observed for the sandstone and carbonate samples. The results for tight-gas sandstones and shales are more diffuse, with values ranging 0.1–1.9. Estimates from the intact and thermally damaged core samples are consistent with other published studies, showing that for intact rock, B_N/B_T is lower than unity and that the range broadens and expands to values higher than unity when the rock is damaged.

ACKNOWLEDGMENTS

We thank ITF and the sponsors of the IPEGG project, British Gas, BP, Statoil, and ENI. We also thank Colin Sayers for an informal discussion of our results during the initial stages of this work as well as Associate Editor Boris Gurevich, Sonja Maultzsch, and three anonymous reviewers for constructive criticism. James Verdon was supported by a UKERC Interdisciplinary Studentship Award. Doug Schmitt is also thanked for providing some of the data from his graduate students.

REFERENCES

Angus, D., J. Verdon, J.-M. Kendall, Q. Fisher, J. Segura, S. Skachkov, M. Dutko, and A. Crook, 2008, Influence of fault transmissibility on seismic attributes based on coupled fluid-flow and geomechanical simulation: 78th Annual International Meeting, SEG, Expanded Abstracts, 1600–1604.

Bakulin, A., I. Tsvankin, and V. Grechka, 2000, Estimation of fracture parameters from reflection seismic data — Part I: HTI model due to a single fracture set: Geophysics, **65**, 1788–1802.

Brown, L., 2002, Integration of rock physics and reservoir simulation for the interpretation of time-lapse seismic data at Weyburn field, Saskatchewan: M.S. thesis, Colorado School of Mines.

Brown, R., and J. Korringa, 1975, On the dependence of the elastic properties of a porous rock on the compressibility of the pore fluid: Geophysics, **40**, 608–616.

Calvert, R., 2005, Insights and methods for 4D reservoir monitoring and characterization: SEG.

Dean, R., X. Gai, C. Stone, and S. Minkoff, 2005, A comparison of techniques for coupling porous flow and geomechanics: Society of Petroleum Engineering Reservoir Simulation Symposium, 79709.

Grechka, V., and M. Kachanov, 2006, Effective elasticity of fractured rocks: The Leading Edge, **25**, 152–155.

Grochau, M., and B. Gurevich, 2008, Investigation of core data reliability to support time-lapse interpretation in Campos basin, Brazil: Geophysics, **73**, no. 2, E59–E65.

Hall, S., J.-M. Kendall, J. Maddock, and Q. Fisher, 2008, Crack density tensor inversion for analysis of changes in rock frame architecture: Geophysical Journal International, **173**, 577–592.

Han, D.-H., 1986, Effects of porosity and clay content on acoustic properties of sandstones and unconsolidated sediments: Ph.D. dissertation, Stanford University.

Hatchell, P., and S. Bourne, 2005, Rocks under strain: Strain-induced time-lapse time shifts are observed for depleting reservoirs: The Leading Edge, **24**, 1222–1225.

He, T., 2006, P- and S-wave velocity measurement and pressure sensitivity analysis of AVA response: M.S. thesis, University of Alberta.

Hemsing, D., 2007, Laboratory determination of seismic anisotropy in sedimentary rock from the Western Canadian Sedimentary Basin: M.S. thesis, University of Alberta.

Herwanger, J., and S. Horne, 2005, Predicting time-lapse stress effects in seismic data: The Leading Edge, **12**, 1234–1242.

Jizba, D., 1991, Mechanical and acoustical properties of sandstones and shales: Ph.D. dissertation, Stanford University.

Johnston, J., and N. Christensen, 1995, Seismic anisotropy of shales: Journal of Geophysical Research, **100**, no. B4, 5991–6003.

Kendall, J.-M., Q. Fisher, S. Crump, J. Maddock, A. Carter, S. Hall, J. Wookey, S. Valcke, M. Casey, G. Lloyd, and W. Ismail, 2007, Seismic anisotropy as an indicator of reservoir quality in siliciclastic rocks: Geological Society of London, Special Publication, **292**, 123–136.

King, M., 1966, Wave velocities in rocks as a function of changes in overburden pressure and pore fluid saturants: Geophysics, **31**, 50–73.

———, 2002, Elastic wave propagation in and permeability for rocks with multiple parallel fractures: International Journal of Rock Mechanics and Mining Sciences, **39**, 1033–1043.

Lubbe, R., J. Sothcott, M. Worthington, and C. McCann, 2007, Laboratory estimates of normal/shear fracture compliance ratio: 69th Annual Conference and Exhibition, EAGE, Extended Abstracts, F026.

———, 2008, Laboratory estimates of normal and shear fracture compliance: Geophysical Prospecting, **56**, 239–247.

MacBeth, C., 2004, A classification for the pressure-sensitivity properties of a sandstone rock frame: Geophysics, **69**, 497–510.

MacBeth, C., and H. Schuett, 2007, The stress dependent elastic properties of thermally induced microfractures in aeolian Rotliegend Sandstone: Geophysical Prospecting, **55**, 323–332.

Maddock, J., 2006, Seismic anisotropy in siliciclastic reservoir rocks: Ph.D. dissertation, University of Leeds.

Nur, A., and G. Simmons, 1969, The effect of saturation on velocity in low porosity rocks: Earth and Planetary Science Letters, **7**, 183–193.

Olden, P., P. Corbett, R. Westerman, J. Somerville, B. Smart, and N. Koutsabeloulis, 2001, Modeling combined fluid and stress change effects in the seismic response of a producing hydrocarbon reservoir: The Leading Edge, **20**, 1154–1163.

Palciauskas, V., 1992, Compressional to shear wave velocity ratio of granular rocks: Role of rough grain contacts: Geophysical Research Letters, **19**, 1683–1686.

Prioul, R., A. Bakulin, and V. Bakulin, 2004, Nonlinear rock physics model for estimation of 3D subsurface stress in anisotropic formations: Theory and laboratory verification: Geophysics, **69**, 415–425.

Raymer, D., A. Tommasi, and J.-M. Kendall, 2000, Predicting the seismic implications of salt anisotropy using numerical simulations of halite deformation: Geophysics, **65**, 1272–1280.

Rojas, M., 2005, Elastic rock properties of tight gas sandstones for reservoir characterization at Rulison field, Colorado: M.S. thesis, Colorado School of Mines.

Sayers, C., 2002, Stress-dependent elastic anisotropy of sandstones: Geophysical Prospecting, **50**, 85–95.

Sayers, C., and D.-H. Han, 2002, The effect of pore fluid on the stress-dependent elastic wave velocities in sandstones: 72nd Annual International Meeting, SEG, Expanded Abstracts, 1842–1845.

Sayers, C., and M. Kachanov, 1995, Microcrack-induced elastic wave anisotropy of brittle rocks: Journal of Geophysical Research, **100**, 4149–4156.

Schoenberg, M., and C. Sayers, 1995, Seismic anisotropy of fractured rock: Geophysics, **60**, 204–211.

Schubnel, A., and Y. Guéguen, 2003, Dispersion and anisotropy of elastic waves in cracked rocks: Journal of Geophysical Research, **108**, no. B2, ESE16.1–ESE16.15.

Shapiro, S., 2003, Elastic piezosensitivity of porous and fractured rocks: Geophysics, **68**, 482–486.

Shapiro, S., and A. Kaselow, 2005, Porosity and elastic anisotropy of rocks under tectonic stress and pore-pressure changes: Geophysics, **70**, no. 5, N27–N38.

Simmons, G., and W. Brace, 1965, Comparison of static and dynamic measurements of compressibility of rocks: Journal of Geophysical Research, **70**, 5649–5656.

Tod, S., 2002, The effects of stress and fluid pressure on the anisotropy of interconnected cracks: Geophysical Journal International, **149**, 149–156.

Valcke, S., M. Casey, G. Lloyd, J.-M. Kendall, and Q. Fisher, 2006, Lattice preferred orientation and seismic anisotropy in sedimentary rocks: Geophysical Journal International, **166**, 652–666.

Van Den Abeele, K. E.-A., J. Carmeliet, P. A. Johnson, and B. Zinszner, 2002, Influence of water saturation on the nonlinear elastic mesoscopic response in earth materials and the implications to the mechanism of nonlinearity: Journal of Geophysical Research, **107**, no. B6, ECV4.1–ECV4.11.

Verdon, J., D. Angus, J.-M. Kendall, and S. Hall, 2008, The effects of microstructure and nonlinear stress on anisotropic seismic velocities: Geophysics, **73**, no. 4, D41–D51.

Walsh, J., 1965a, The effect of cracks on the compressibility of rock: Journal of Geophysical Research, **70**, 381–389.

———, 1965b, The effect of cracks on the uniaxial elastic compression of rocks: Journal of Geophysical Research, **70**, 399–411.

Worthington, M., 2008, Interpreting seismic anisotropy in fractured reservoirs: First Break, **26**, 29–35.

Zimmerman, R., W. Somerton, and M. King, 1986, Compressibility of porous rocks: Journal of Geophysical Research, **91**, 12765–12777.